





# State of the Art of High-Flux Compton/Thomson X-rays Sources

Vittoria Petrillo <sup>1,2,\*</sup>, Illya Drebot <sup>1,†</sup>, Marcel Ruijter <sup>1,†</sup>, Sanae Samsam <sup>1,†</sup>, Alberto Bacci <sup>1</sup>, Camilla Curatolo <sup>1</sup>, Michele Opromolla <sup>1,2</sup> , Marcello Rossetti Conti <sup>1</sup> , Andrea Renato Rossi <sup>1</sup>  and Luca Serafini <sup>1,†</sup> 

<sup>1</sup> INFN-Section of Milan, Via Celoria, 16, 20133 Milano, Italy

<sup>2</sup> Dipartimento di Fisica, Università degli Studi di Milano, Via Celoria, 16, 20133 Milano, Italy

\* Correspondence: vittoria.petrillo@mi.infn.it

† These authors contributed equally to this work.

**Abstract:** In this paper, we present the generalities of the Compton interaction process; we analyse the different paradigms of Inverse Compton Sources, implemented or in commissioning phase at various facilities, or proposed as future projects. We present an overview of the state of the art, with a discussion of the most demanding challenges.

**Keywords:** thomson scattering; compton scattering; synchrotron radiation, X-rays; radiation sources

## 1. Introduction

Thomson/Compton Sources generate energetic and collimated photons through the homonym back-scattering process taking place between high brightness electron beams and high intensity radiation pulses. They basically consist in miniature electron-photon colliders and exploit the large blue-shift imparted to the pump input photons by double relativistic Doppler effect for promoting the photon energy to the X-ray range of about  $E_X = 4\gamma^2 E_L / (1 + \gamma^2 \theta^2)$ , where  $\theta$  is the observer angle,  $E_L$  is the input pump photon energy delivered in most cases by a laser and  $\gamma$  the electron Lorentz factor. When the parameter  $4E_L \gamma / mc^2 \ll 1$ , the recoil of the electrons in their own rest frame is unessential. In this case, the Compton elastic scattering can be treated within the classical electrodynamics, neglecting quantum effects. The production of Compton radiation falls in the examples of interaction of charged particles with external electromagnetic fields, like synchrotron or undulator radiation. In this classical case, the Inverse Compton Sources (ICSs) should be referred to as Thomson Sources. When the input pump photons are in the optical range, this regime occurs typically for electron energies below about 100 MeV ( $\gamma \simeq 200$ ), with X-ray output energies lower than 200 keV. However, following the usual lexicon adopted in the literature, we will use ICS (Inverse Compton Source) for both regimes, even if the device operates in the classical range. Such an useful and promising “photon accelerator” scheme is unfortunately limited by the low efficiency of the back-scattering process in the transformation of the laser photons into X-ray photons. The cross section of Thomson/Compton back-scattering is indeed very small, about  $6 \cdot 10^{-29} \text{ m}^2$ , so a high luminosity collider is needed for generating intense X-ray beams: the luminosity needed to achieve an operating regime where almost each electron converts to X-ray at least one laser pump photon should exceed the one of large colliders, like LHC! This entails the necessity to drive in the interaction region extremely dense laser and electron beams. The production of intense laser pulses and high brightness electron beams with these tight requirements is now state of the art. In ICS sources, therefore, the most important challenge is to synchronize the electron-photon collisions in a controllable and stable manner, in order to deliver to the users tunable, reliable and stable X-ray beams, as it is routinely achieved in the operation of synchrotron light sources. Synchrotrons deliver to users a flux whose intensity ranges between  $10^{14}$  and  $10^{19}$  photons/( $\text{m}^2\text{s}$  0.1% bw) with a spatial coherence length of 1–50  $\mu\text{m}$ . The comparison in performances between various kinds of X-rays sources [1]



**Citation:** Petrillo, V.; Drebot, I.; Ruijter, M.; Samsam, S.; Bacci, A.; Curatolo, C.; Opromolla, M.; Conti, M.R.; Rossi, A.R.; Serafini, L. State of the Art of High-Flux Compton/Thomson X-rays Sources. *Appl. Sci.* **2023**, *13*, 752. <https://doi.org/10.3390/app13020752>

Academic Editor: Saulius Juodkazis

Received: 4 December 2022

Revised: 23 December 2022

Accepted: 27 December 2022

Published: 5 January 2023



**Copyright:** © 2023 by the authors. Licensee MDPI, Basel, Switzerland. This article is an open access article distributed under the terms and conditions of the Creative Commons Attribution (CC BY) license (<https://creativecommons.org/licenses/by/4.0/>).

shows that microfocus X-ray tubes deliver  $2 \cdot 10^2$ – $2 \cdot 10^6$  photons/(m<sup>2</sup>s 0.1% bw) with a spatial coherence length of  $10^{-1}$ – $5 \mu\text{m}$ , while metal jet X-ray tubes produce  $5 \cdot 10^5$ – $2 \cdot 10^8$  photons/(m<sup>2</sup>s 0.1% bw) with a corresponding spatial coherence length of  $4 \cdot 10^{-1}$ – $5 \mu\text{m}$ . A larger flux between  $10^5$  and  $10^9$  photons/(m<sup>2</sup>s 0.1% bw) is achieved with static anode X-ray tubes, while the rotating anode X-ray tubes provide  $10^6$ – $10^{10}$  photons/(m<sup>2</sup>s 0.1% bw), both with  $2 \cdot 10^{-3}$ – $10^{-1} \mu\text{m}$  of spatial coherence length. Inverse Compton Scattering sources generate a flux with intensity from  $10^{10}$  to  $10^{13}$  photons/(m<sup>2</sup>s 0.1% bw), intermediate between tubes and synchrotron sources, with the largest spatial coherence lengths of 5–100  $\mu\text{m}$ . Respect to these last huge facilities, ICS sources guaranty high energetic sustainability and compact footprint, permitting the lowest cost per single X-ray photon. Tens of devices of this kind have been commissioned in the last twenty-five years [2–12], several of them operating nowadays as test and user facilities. Most of the existing Compton devices are actually devoted either to experiments on the radiation characterization [10,13–17], test of imaging techniques [18–21] or to radiological applications on biological, animal and human samples [6,22–25].  $\gamma$  rays have been detected at [26] and routinely produced at the Hi $\gamma$ s facility [12]. Moreover, several advanced projects have been developed in the last years [27–38]. An additional advantage of Compton sources is the large degree of freedom due to the operation with laser pulses, instead of magnetic elements. The optical technology of pulse manipulation permits in principle to adapt the laser signal to the needs of the users, stimulating at the same time various theoretical research lines [39–47]. The versatility in shaping the frequency laser pulse distribution has been exploited for compensating the non-linear spectral deterioration with chirping [42–44] or with polarization gating, for mitigating the bandwidth broadening due to energy spread by chirping [46,47], for the control of higher harmonics [48,49], while a temporal modulated electron bunch has been shown to produce coherent emission [50]. Proposals for using the Compton light as diagnostics for the electron beam are also ongoing [51,52]. Regarding the operational possibilities, different possible schemes there exist. Since accelerated electrons can be obtained with storage ring as well as in warm or energy recovery linacs, and, on the other hand, there are two categories for high power lasers, resonators and chirped pulse amplification (CPA), the ICS sources can be grouped in few main paradigms: (i) RF Photo-injector producing a high charge electron bunch against a  $J$ -class laser pulse, strongly focused, running collisions at low repetition rate [2,5–7,27,35]. (ii) Moderately high charge electron beam, generated at high repetition rate in a Compact Storage Ring with a  $mJ$ -class laser pulse stored in an optical Fabry-Pérot Cavity, tightly focused [8,9,26,28,30,53]. (iii) Low charge electron bunch delivered at very high repetition rate by a Super-Conducting RF Photo-Injector colliding with a  $mJ$ -class laser pulse stored in an optical Fabry-Perot Cavity (up to 1 MW stored laser power), focused at collision [29,33,34,37,38]. In addition, several exotic schemes have been conceived or implemented, including plasma accelerated beams for ultra-compact devices [11,54], Free-Electron lasers [12,55] or Terahertz radiation [56] as input pump instead of lasers, sophisticate or extreme laser structures allowing coherent radiation generation or two frequency operation [57–60]. In this paper, after a section where we discuss generalities on the Compton interaction, we will analyse the main paradigms of ICS sources, operating either in the classical or in the quantum regime; then we will give an overview of the state of the art, going into details in few specific examples.

## 2. Generalities on Thomson/Compton Scattering

In boosted sources, the radiation frequency depends on the electron Lorentz factor  $\gamma$ , on the observer position  $\theta$ , on the input pump frequency  $\omega_L$  and on the interaction angle  $\alpha$  according to:

$$\omega_X = \frac{\omega_L(1 + \cos \alpha)}{(1 - \beta \cos \theta + 2\hbar\omega_L/(mc^2\gamma))}. \quad (1)$$

This expression, where  $\hbar$  is the reduced Planck constant,  $\beta = v_e/c$ ,  $v_e$  being the electron velocity,  $c$  the speed of light and  $m$  the electron mass, shows the frequency-angle correlation

due to the boost which concentrates the highest energy photons at the center of the pulse, while the less energetic photons occupy the outer zone. In the limit  $4h \omega_L \gamma / (mc^2) \ll 1$  the last term in the denominator is negligible and the process is classical.

The total achievable X-ray flux is approximately given for head-on collision ( $\alpha = 0$ ) by:

$$N_x \approx \sigma_{Th} f_{RF} \frac{N_e N_L}{2\pi(\sigma_e^2 + \sigma_L^2)} \tag{2}$$

where  $\sigma_{Th} = 6.65 \times 10^{-29} m^2$  is the Thomson cross section,  $N_e = Q/e = 6.25 \times 10^9 Q(nC)$ ,  $N_L = E_L / (h\nu_L) = E_L \lambda_L / (hc) \simeq 5 \times 10^{24} E_L(J) \lambda_L(m)$  is the number of laser photons,  $f_{RF}$  the repetition rate of the system and  $\sigma_L$  and  $\sigma_e$  are the rms transverse dimension of the laser and electron distribution, respectively.

The rms X-ray beam bandwidth  $bw$ , in the linear approach, is approximately given by [61,62]:

$$bw \approx \sqrt{\left[ \frac{\Psi^2 / \sqrt{12}}{1 + \Psi^2 / 2} + \frac{2\varepsilon_n^2}{\sigma_e^2} \right]^2 + \left[ 2 \frac{\Delta\gamma}{\langle \gamma \rangle} \right]^2 + \left[ \frac{\Delta\omega_L}{\omega_L} \right]^2 + \left[ \frac{M^2 \lambda}{4\pi\sigma_L} \right]^4} \tag{3}$$

where the acceptance  $\Psi = \gamma\theta_{acc}$  scales with the collimation angle  $\theta_{acc}$ ,  $\varepsilon_n$  is the emittance of the electron beam,  $\frac{\Delta\omega_L}{\omega_L}$  the proper rms bandwidth of the laser and  $M$  its purity factor. The number of X-ray photons produced per second in a given rms bandwidth  $bw$  and collected within a collimation forward angle  $\theta_{acc}$ , given in practical units, is:

$$N_{x,bw} \approx 5.8 \times 10^{11} f_{RF} \frac{E_L(J)Q(nC)}{\sigma_x^2(\mu m^2)} \gamma^2 \theta_{acc}^2 \tag{4}$$

where, for the sake of simplicity, both laser and electron beams are supposed to arrive at the interaction point (IP) with rms transverse sizes  $\sigma_x$ .

The polarization properties of the Compton radiation follow those of the laser, so linear polarized lasers generate mainly linear polarized X-rays, while circular polarized lasers induce circular polarization. At the outer border, a crown of radiation characterized by different polarization occurs, due to the formation of the relativistic cone. The effect is weak and usually involves few photons [63]. The longitudinal coherence is extremely scarce. On the transverse plane, however, due to the small radius of the source, coherence areas of linear dimension in the micron range and widening during propagation occur. This structure can be exploited in phase contrast imaging. In the mild non-linear regime, where the laser parameter  $a_0 = eE_0 / (mc\omega_L)$  is order or larger than 1 ( $E_0$  and  $\omega_L$  being the peak electric field and the angular frequency of the laser pulse, respectively), the bandwidth presents a shift of the peak towards lower frequency values, the occurrence of spectral fluctuations and an ample broadening due to non-linear multi-photon effects in the back-scattering [4,64–66], followed by the insurgence of the harmonics, whose characteristics have been detected and studied [67]. The use of high intensity ultra short laser systems as interaction laser presents therefore serious limitations. Sophisticated schemes relying on laser chirp have been proposed in order to compensate the non-linear broadening while maintaining the spectral flux [39,43,44]. Another peculiar characteristics that can be carried by the radiation is the orbital momentum that can be transferred to it either by the electron beam or by the laser pulse [68].

### 3. Discussion of Different Paradigms: Low Energy Sources Operating in Classical Regime

As a reference value for applications in the medical field, radiological images are so far currently performed by Roentgen X-ray tubes with fluxes from at least  $10^{11}$  up to  $10^{12}$  X-ray photons/s, with the typical broad-band spectrum ( $bw > 40\%$ ) of the bremsstrahlung radiation. The objective for Compton devices voted to imaging experiments is to achieve similar fluxes but with the quasi-monochromatic X-ray spectrum ( $bw \simeq 10\%$ ) of the ICSs. Nuclear photonics applications, on the other hand, require photon energies in the MeV

range and relative bandwidths of the order of few  $10^{-3}$ . The basic criteria for reaching such large fluxes and high spectral densities can be deduced from Equations (3) and (4). We can distinguish the ICS configurations in two classes according to the value of  $f_{RF}$ , namely  $f_{RF}$  up to 100 Hz, as occurring in warm linacs, and  $f_{RF}$  of the order or larger than 1 MHz as in storage rings or Energy Recovery Linacs (ERLs). In the first case of low repetition rates, the flux should be maximized by increasing the number of electrons, namely the charge, the number of photons, i.e. the laser energy, and by focusing tightly the beams. In this case, it is clearly evident the need of high brightness electron beams, carrying high charge bunches at low emittance and energy spread, combined with lasers delivering high energy, picosecond long pulses with small bandwidth and high mode purity ( $M^2 \simeq 1$ ). In this way, the X-ray bandwidth will take advantage of the beam quality and could reach particularly low values (relative values down to  $5 \times 10^{-3}$ ), thus making this paradigm suitable even for nuclear photonic applications. The former requirements point clearly to electron accelerators similar to those projected for alimending Free Electron Lasers. If the repetition rate is larger by a factor  $10^6$  with respect to the previous case of warm linacs, large photon fluxes can be reached also if the single shot electron number is not as large as the case before, if the pump energy is low or the focusing is not so strict. This latter situation requires laser systems capable of high repetition rate and large average power, combined to short pulses and mode-locking to assure synchronization at the sub-picosecond level between the electron beam and the laser pulse at the Interaction Point. The large repetition rate can be obtained by electron beams generated both with storage ring or Super-Conducting (SC) linacs, with or without energy recovery, colliding with laser pulses stored in Fabry-Pèrot cavities. Electron beams in storage rings are characterized by unexceptional quality, limiting the bandwidth narrowness and the spectral density that can be achieved. Super-Conducting linacs, on the other hand, generate low charge beamlets. In both cases, the focusing of the laser pulse is dominated by the cavity geometry and the spot in the IP could be not so reduced as in free space.

Presently there are therefore three main paradigms for high performance ICS working in a low energy regime (electron energy less than 100 MeV):

### 3.1. (i) Warm Linac + Single Shot Laser

The first group of ICSs is constituted by RF Photo-injector producing a high charge up to 1–2 nC electron bunch against a *J*-class laser pulse delivered by an amplified laser system (Ti:Sa, Yb:Yag or CO<sub>2</sub>), colliding at a repetition rate of 1–100 Hz, with the beams tightly focused down to 10–40  $\mu\text{m}$ . The possibility of reaching such small spot sizes is due to the low beam emittance and energy spread achievable thanks to high gradient RF fields in the accelerator and to the fact that the electron beam is not recirculated but dumped after each collision. The same holds for the laser operated in single shot pulses, with energy values up to 5–7 J. The main drawback of this archetype is the low repetition rate achievable, approaching 100 Hz in the present state of the art, limited by both RF and by collision laser capabilities. Laser recirculators, that could enhance the repetition rate by a factor 30–40 [69], has been developed but are still to be diffused and routinely used. The enhancement to 40 Hz of the low repetition rate CO<sub>2</sub> laser has been performed at BNL [70]. This paradigm has been widely explored theoretically and exploited experimentally with tens of sources commissioned or still operating and tens of projects. After first pioneering attempts [3], best examples of this model are ATF at BNL [2], a pivotal ICS with more than tens years of operation and applications spread in all fields; Sparc [5], commissioned at LNF-Frascati; TTX [7] at Tsinghua and Aist [6] in Japan, infrastructures with a long cursus of experiments and currently still working; as well as STAR (Southern Europe Thomson source for Applied Research) [35], a dedicated user facility in construction at the University of Calabria (Italy). Figure 1 shows the typical scheme of such machines. In particular, the figure refers to the STAR source [36]. The device is hosted into a 2.5 m wall bunker and consists of an RF S-band photo-injector, which generates 5 MeV electron bunches, at 100 Hz repetition rate; two electron lines, low energy and high energy, alimended by an S-band linear accelerator

(LINAC) which accelerates the electron bunches up to 60 MeV, both driven by a 55 MW RF pulsed modulator; focusing devices (quadrupoles and steering magnets); diagnostic devices (beam current monitors, beam position monitors, YAG screens); two lasers (one UV photo-cathode laser and a IR interaction laser), hosted into a dedicated clean room. A dogleg introduces an offset between the linac and the interaction point rerouting the background due to the dark current. The quasi-monochromatic polarized radiation will be tunable with continuity from 10 to 140 keV, just increasing the electron energy. At the phase I of the project, an X-ray flux of about  $10^9$  photons per second within a 10% bandwidth is expected, with picosecond-class pulse length. In Table 1 the electron beam and laser characteristics, the photon energy and the fluxes achieved by several of these devices (measured or predicted) are summarized.

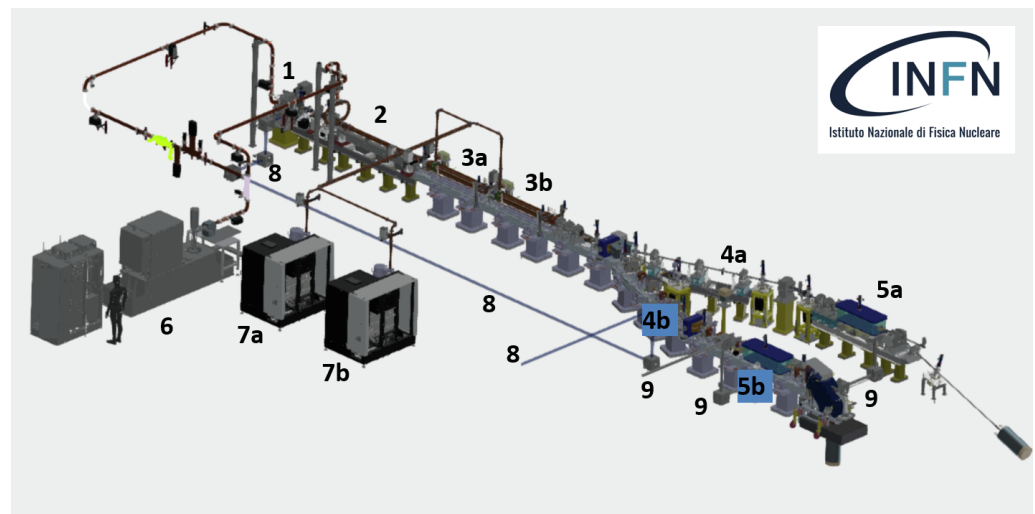


**Figure 1.** STAR machine as an example of Paradigm (i). Overall length about 12 m. 1: S-band RF Gun; 2: S-band Accelerating section; 3a,b: C-band Accelerating sections, 4a,b: low energy and high energy beam transport lines; 5a,b: low energy and high energy interaction chambers; 6: S-band RF power station; 7a,b: C-band RF power stations; 8: photo-cathode laser transport line; 9: interaction laser transport line. Courtesy of L. Pellegrino.

**Table 1.** Warm linacs versus high-energy laser. The number of photons is per shot. All data are measured apart the case of STAR, whose data are evaluated numerically.

ICS	Electron Energy (MeV)	$\lambda_{las}$ ( $\mu\text{m}$ )	Laser Energy (J)	X Energy (keV)	X Flux	Bandwidth	Rep. Rate (Hz)
BNL [2]	64–72	10	2	7–8.9	$2 \cdot 10^8$	<5%	<10
T-ReX [4]	116	0.532	0.15	0.1–0.9	$10^5$	15%	10
Sparc [5]	30	0.8	5	13	$1.4 \cdot 10^6$	20%	10
AIST [6]	42	0.8	0.14	40	$10^6$	4–10%	10
TTX [7]	46.7	0.8	0.3	51.7	$10^6$	10%	100
Elbe [10]	23	0.8	2.25	13–25		25%	10
STAR-II-HE [35]	140	1.03	0.5	350	$10^7$	6%	100

In the hard X-ray range, in situations where the photon energy is roughly between ten and few hundreds keV,  $10^5$ – $10^8$  photons per shot are generated, a number that can mean  $10^7$ – $10^{10}$  photons/s, taking into account the repetition rate of the scattering. Since this paradigm can provide intense single radiation shots not affected by beam fluctuations, it is particularly suitable for studying the radiation characteristics. Much of the run time of these machines has been dedicated to these tests. The energy-angle correlation,



described in Equation (1), has been validated at HDMZ by shifting horizontally the detector [13], using diffraction based method [71], by means of filters with different K-edge energies [18,72] or by producing a direct frequency-angle map [16] with a sophisticated spectrometer. Polarization control has been studied at Tsinghua with a cylindrical detector collecting the radiation [73]. The production of X rays with elliptical polarization and their detection [21] has been demonstrated in a single shot device based on plasma accelerated electron beams [11]. The generation of radiation with orbital momentum has also been tried [74]. The dependence of spectral properties on emittance and laser parameter have been analysed in various conditions [10] by appositely deteriorating the electron beam for increasing the emittance, while changing the laser intensity. Occurrence, structure and polarization of the harmonics have been observed at BNL [2]. Applications involving users foreseen for this group of machines fall mostly in the imaging field. Lot of experiments have been done along this line. At AIST, microfractures in human bones have been detected [23], as well as microvessels in animal models for microangiography [75] and rat lumbar vertebrae [76]. At BNL the radiography of a wasp done with the phase contrast technique [22]. The set up can be easily upgraded in energy by adding more RF accelerating structures. The high electron beam quality (emittance less than 1 mm mrad and relative energy spread approaching  $10^{-4}$ ) permit also to get down the bandwidth to few  $10^{-3}$  satisfying the requirements of the nuclear photonics applications.

### 3.2. (ii) Storage Ring + Laser in Cavity

The second paradigm relies on Compact Storage Ring for the electron beam, colliding a mildly high charge electron bunch with a mJ-class laser pulse stored in an optical Fabry-Perot Cavity, at the large repetition rate of up to 25 MHz, (connected to an average beam current of 15 mA), with a focus of 50–150  $\mu\text{m}$  spot size at collision. This paradigm is at the basis of the most productive ICS actually existing [8,9]. Figure 2 shows the typical scheme of a source based on it. The overall length is of order of ten meters with a surface size of about  $10^2 \text{ m}^2$ .

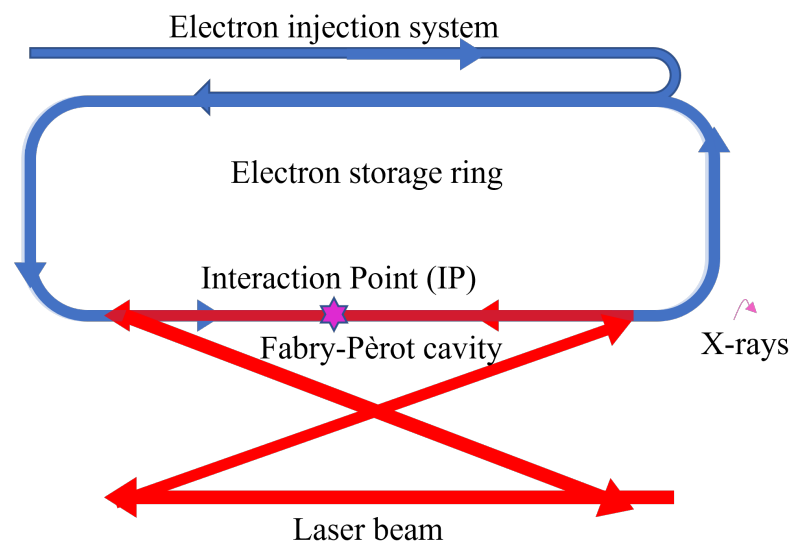


**Figure 2.** The typical scheme of source based on Paradigm (ii). Size is about  $100 \text{ m}^2$ . Overall length about 12 m.

An injection system drives the electron beam produced by a gun and accelerated by a short linac into a storage ring. The beam is necessarily coupled with a laser pulse in cavity in a region of zero dispersion. The laser in Fabry-Pèrot cavity is characterized by pulses carrying low energy in each passage in the cavity and produce therefore few X photons per interaction. The advantage of this paradigm is the high repetition rate connected to the storage of the electron beam in a ring, making it particularly suitable to the

applications requiring high statistics. On the other hand, the beam instabilities developing in the propagation in the ring at low energies (50 MeV) impede the tight focusing of the beam at IP. Pulsed operation is also quite hard to implement. The best example of this category is CLS, which has been commercially developed and manufactured by Lyncean Technologies, Inc (Palo Alto, CA, USA). It was commissioned first at Palo Alto (named there CLS), while now is operating at Munich as MUCLS. Its best performances are a maximum photon flux of  $5 \cdot 10^{10}$  with a maximum photon energy of 35 keV. At Palo Alto, insects and seeds have been first detected with a grating interferometer for differential phase-contrast imaging, producing contemporary absorption, phase contrast and dark field images [8]. Then, slices of mice lungs have been studied for diagnosing and mapping the pulmonary emphysema [77,78]. Benchmark tests of X-ray diffraction data collection with hen egg white lysozyme, and successful high-resolution X-ray structure determination of the Glycine cleavage system protein H from Mycobacterium tuberculosis using diffraction data has also been done [79]. Great attention was also paid to the development of tomographic techniques [80]. Then the device was shifted at Munich, where, as MUCLS, was operated for producing in-vivo images. Pig chests [81] or mouse lungs [82] have been detected, paving the road to human lung in-vivo observation [83]. X-ray absorption spectroscopy of a Ag foil has been performed [84], developing an ad hoc technique which exploits the large repetition rate of the source. Demonstration of more sophisticated imaging techniques have also been performed [85], as well as the microbeam radiation therapy [86]. Another example of storage ring based ICS is ThomX [28], in commissioning at Orsay-LAL by a collaboration IN2P3-Universit  de Paris Sud, that will be dedicated to applications in the field of the conservation of the cultural heritage in cooperation with the Museum Louvre. Table 2 summarizes typical parameters of these sources.

**Table 2.** Storage ring+ laser in Fabry-P rot cavity. The data of CLS and MUCLS are measured, the ThomX data are estimated.

ICS	Electron Energy (MeV)	$\lambda_{las}$ ( $\mu\text{m}$ )	Laser Energy (mJ)	X Energy (keV)	X Flux	Bandwidth	Rep. Rate (Hz)
CLS [8]	25–45	1	5	8–42	$5 \cdot 10^2 - 5 \cdot 10^3$	3%	$65 \cdot 10^6$
MUCLS [9]	25–45	1	5	8–42	$5 \cdot 10^2 - 5 \cdot 10^3$	3–5%	$65 \cdot 10^6$
ThomX [28]	50	1.03	$1.4 - 2.6 \cdot 10^{-3}$	45	$10^5$	10%	$65 \cdot 10^6$

### 3.3. (iii) Superconducting Linac + Laser in Cavity

This paradigm relies on Super-Conducting RF Photo-Injector delivering a low charge electron bunch (tens of pC) at a very large repetition rate (up to 100 MHz), colliding with a mJ-class laser in cavity. The laser pulse, stored in an optical Fabry-Perot Cavity, with up to 1 MW stored laser power, is focused to 20–30  $\mu\text{m}$  spot size at collision. Linacs based on superconducting cavities can present the extremely interesting option of recovering the electron energy in a stage downstream the ICS interaction point. While several accelerators based on SuperConducting Linacs (with or without the energy recovery) are already operating and other projects are in various stages of commissioning, Compton sources driven by SC linacs are so far not yet completed, apart for some experimental tests of X-ray production made by cERL at KEK [31]. There are however several projects, estimating ICS performances. The achieved maximum photon energy is 200 keV. The maximum achievable fluxes is estimated to be  $3.5 \cdot 10^{12}$  photons/s without energy recovery with an average electron beam current 1 mA, while in excess of an impressive  $10^{15}$  with energy recovery at an average electron current of about 100 mA. Proposals based on this paradigm are UH-FLUX [33] in development in UK and presenting the option of the energy recovery, CBeta [29], bERLinPro [34], CLXS [32], an ongoing project at MIT (without energy recovery), BriXS [37] based on two injectors similar to the original scheme by Tigner [87] and BriXSinO [38], that is instead a demonstrator for BriXS and is in the building phase at LASA INFN Laboratory at Milan. Combining the typical operation made with a linac, where the beam is dumped after the

collision at IP, with the high repetition rate typical of a storage ring (from tens to hundreds MHz) constitutes the appealing characteristic of paradigm (iii). This is possible thanks to the operation with the super-conducting RF cavities accelerating the electron beam. In case of energy recovery, the average electron beam current can arrive to exceed 20 mA, a value representing the maximum level for storage rings of paradigm (ii) when operated at low electron energy (about 50 MeV typically for an ICS, compared to 1–5 GeV of synchrotrons), approaching 100 mA, comparable to synchrotron light sources. For this paradigm one challenge is the electron beam injector, in particular the reachable average electron beam current associated the overall good beam quality, such as low emittance and energy spread. As an example of paradigm (iii), Figure 3 shows a rendering with the scheme of BriXSinO. After the injector, a dogleg introduces an offset between the photocathode and the super-conducting cavities. Downstream the linac, a ring brings back the electron beam to the end of the linac for the second passage. The arc, constituted by a suitable number of Double Bending Achromats (DBA) is also able to compress the electron beam, a feature useful in the FEL operation. The zero dispersion zones between the achromats host insertion devices. In one branch a FEL oscillator delivering Terahertz radiation is foreseen, in another one the ICS takes place. A Laser in Fabry-Pèrot cavity will permit one or two color operation [60]. The line is equipped with focusing systems and diagnostics. The superconducting cavities can be operated in the two-pass two-way conditions, either for doubling the energy or for energy recovery. Contained dimensions and expenses and the energy recovery operation make minimum the cost per photon and maximum the sustainability of this device option. Present state of the art of the average current in ERL photo-injectors is about 10 mA [88], but several projects world-wide aim at 100 mA and above [89].

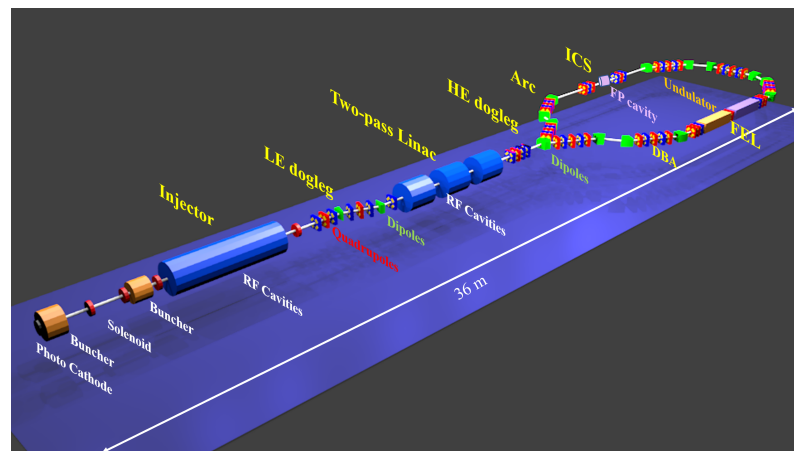


**Figure 3.** BriXSinO as an example of Paradigm (iii) with energy recovery (average electron beam current up to 8 mA).

Table 3 summarizes typical parameters of these sources.



**Table 3.** ERL +laser in cavity. All data are estimated, apart the KEK data, that are measured.

ICS	Electron Energy (MeV)	$\lambda_{las}$ ( $\mu\text{m}$ )	Laser Energy (mJ)	X Energy (keV)	X/Shot	Bandwidth	Rep. Rate (Hz)	X/s
UH-FLUX [33]	20	1		15	$2 \cdot 10^4$	0.1%	$1.3 \cdot 10^9$	$2 \cdot 10^{13}$
CBETA [29]	42–150	1.06	$6.2 \cdot 10^{-2}$	32–402	$2 \cdot 10^2$	>10%	$1.62 \cdot 10^8$	$3 \cdot 10^{10}$
bERLinPro [34]	30	0.8		20				
CXLS [32]	8–40	0.515	50	12.4	$5 \cdot 10^6$	5%	$10^5$	$5 \cdot 10^{11}$
KEK [31]	20	1.064	0.064	6.96	$3.01 \cdot 10^3$	3%	$1.62 \cdot 10^8$	$5 \cdot 10^{11}$
BriXS [37]	30–100	1.03	7.5	20–180	$0.05\text{--}1 \cdot 10^5$	0.1–1%	$10^8$	$0.05\text{--}1 \cdot 10^{13}$
BriXSinO [38]	<80	1.03	2.7	30–35	$1\text{--}10 \cdot 10^3$	2–10%	$10^8$	$0.1\text{--}1 \cdot 10^{12}$

For this last paradigm, the X-ray flux achievable can be also expressed approximately in terms of the average electron beam current  $I_e$ , laser power  $P_{FP}$  stored in the Fabry-Perot cavity and effective repetition rate of collisions  $f_{FP}$  as :

$$N_{X,bw} \approx 1.4 \times 10^{17} \gamma^2 \theta^2 P_{FP}(\text{MeV}) I_e(\text{mA}) f_{FP}(\text{MHz}) \frac{\sigma_x^2(\mu\text{m}) Q(\text{nC})}{\sigma_x^2(\mu\text{m}^2)} \gamma^2 \theta_{acc}^2. \quad (5)$$

This formula shows that only the projects BriXS and UHFLUX could reach and even overcome the flux of synchrotrons, this occurring when the average current achieves 100 mA, and the laser power stored in the Fabry-Perot optical cavity exceeds 1 MW.

In all the three paradigms introduced above, the sources deliver sequences of picosecond long X-ray radiation bursts (shorter than the ones produced by synchrotrons) with polarization completely controlled from linear to circular or elliptical. Moreover, the small dimension and the round shape of the emitting source, with radii in the range of 10–80  $\mu\text{m}$ , increasing the local transverse coherence of the radiation beam, makes possible to exploit the effect edge enhancement needed in phase contrast techniques. The coherence areas, moreover, expand as  $\lambda L / \sigma^2$  after propagating a significant length  $L$  from the source to the end user, with  $L$  typically of the order of few tens of meters. This is a key issue for advanced radiological imaging applications.

The advantages of parading (i) derives from the low value of beam emittance that can be achieved thanks to the high gradient of the radiofrequency field maintained in the cavities of the accelerator and to the fact that the electron beam is dumped and restored after each collision. This permits to converge the electron beam at IP to foci of sizes of the order of 10–20  $\mu\text{m}$  and to exploit also the focusing possible for a single pulse laser. Main drawback of this paradigm is the intrinsic limitation of the repetition rate achievable, about 100 Hz in the present state of the art. Same considerations hold for the laser pulse, except for the possible option of a laser recirculator (a device experimentally implemented, but not yet tested on ICS facilities) that multiplies at each RF pulse the collision number by a significant factor. The repetition rate of the source could raise from 100 Hz to a few kHz, enhancing, in turn, the effective X-ray flux to the end user. The machine could also be easily upgraded in energy by adding more RF accelerating modules so that nuclear photon energies larger than 20 MeV can be achieved by ICS based on this paradigm with GeV-class warm Linacs, like the one described in the EuroGammas proposal. Sophisticated techniques, like laser chirping, tilting or modulation could be tested for incrementing the spectral flux. Paradigm (ii) presents the advantage of the high repetition rate associated to the storage of the electrons in a ring. The beam instabilities in this configuration at low energies (50 MeV) impede, however, to focus tightly the beam at IP. The laser is necessarily a system in Fabry-Pèrot cavity, characterized by low single-passage energy and transverse sizes of order of 50–100  $\mu\text{m}$ . The use of a double cavity could permit a double color operation. On the other hand, the implementation of pulsed operations is hard. The upgrade in energy is also an issue, since it entails to re-design the whole machine. Paradigm (iii) has the

appealing characteristics of combining the beam quality typical of operation with a warm Linac with the high repetition rate of a storage ring (tens up to hundreds of MHz) due to the operation with the super-conducting RF cavities used to accelerate the electron beam. The energy recovery permits to overpass 20 mA of average electron beam current, a value that represents the maximum level for storage rings operated at the low electron energies of about 50 MeV. The average current could even be pushed to 100 mA, a value that can be comparable to that used in Synchrotrons operating at 1–5 GeV of energy. One of the main challenge of this system is the performance of the electron beam injector, in particular the achievable average electron beam current associated to small emittance and overall good beam quality. The use of big cryogenic systems increases the complexity of the structure. All this projects has been conceived in the context of a broad spectrum inter-disciplinary large research infrastructure aiming at delivering advanced beams of electrons, photons, neutrons and positrons for basic and applied physics.

#### 4. Discussion of Different Paradigms: High Energy Sources Operating in Quantum Regime

Increasing the electron energy and the pump photon energy  $\gamma$ -rays can be generated. The recoil factor, that in the case of low energy Compton sources was order or below  $10^{-3}$  and therefore completely negligible, in this case is larger than this value, and begins to influence the spectrum emitted, shifting the peak towards lower energy value. At the same time, the cross section diminishes, lowering the flux. One of the most interesting example of applications with  $\gamma$ -rays is the non-destructive isotope imaging by measuring nuclear resonance fluorescence (NRF) [90]. In the experiment, done at the TERAS facility, then damaged by the 2011 earthquake, the quasi-three dimensional distribution of  $^{208}\text{Pb}$  was identified by measuring the amount of 5512 MeV  $\gamma$ -rays which were emitted from  $^{208}\text{Pb}$  via the NRF process. As a matter of fact, high energy photons generated by ICS can be useful for testing nuclear transitions with MeV-class energies, even in excess of 20 MeV. Many pioneering experiments shown the generation of  $\gamma$ -rays of few/tens MeV via Compton back-scattering [91–94] between Infrared lasers and electrons in storage rings. At the NewSUBARU line at SPRING-8 the interaction between a GeV-class electron beam with Nd and CO<sub>2</sub> lasers produced up to  $5 \cdot 10^6$  photon at 17–37 MeV [95]. The UVSOR-III ICS gamma source works also in this regime, providing collisions between the electron beam produced with the homonym storage ring and a 1.94  $\mu\text{m}$  laser, with an output of up to  $10^7$  gamma photons at 5.4 MeV [30]. This paradigm have been exploited even to generate GeV-class photons. At the LEPS beamline, ultraviolet (UV) laser light with a wavelength of 355 nm is injected into SPring-8 to produce a  $10^6$  photons/s beam in the energy range up to 2.4 GeV [96], with the idea to increase further photon energy and flux with a new 266 nm laser line [97]. Free-electron laser oscillators for Ultra-Violet and Vacuum Ultra-Violet have also been employed as Compton photon sources for MeV  $\gamma$ -rays. An interesting option is the interaction between the Free-electron laser light and a positron beam, proved at ACO [98]. A flux of  $2.5 \cdot 10^5$  ph/s of  $\gamma$ -rays at 3 MeV has been generated at NewSUBARU [26]; gamma rays of 14.6 and 25.2 MeV have been generated at UVSOR-III [99], while  $2 \cdot 10^5$  ph/s at 12 MeV have been observed at DUKE [92,100]. A nearly monochromatic beam of 100% linearly polarized  $\gamma$  rays has been produced via Compton backscattering inside a free electron laser optical cavity. 12.2 MeV  $\gamma$  rays were obtained by backscattering 379.4 nm free-electron laser photons from 500 MeV electrons circulating in a storage ring [101]. The experience at Duke has evolved in the high intensity  $\gamma$ -ray source (HI $\gamma$ S), representing, with its flux of  $10^{10}$  ph/s, indeed, the state of the art of  $\gamma$  Compton sources. HI $\gamma$ S is based on Compton scattering of UV photons generated in a FEL oscillator by electrons at a 1.2 GeV storage ring. The  $\gamma$ -ray source routinely provides quasi-monochromatic photons at 1–100 MeV [12]. A different concept of gamma ray source is based instead on the first paradigm. A warm linac implemented up to 700 MeV and a Nd-Yag laser empowered by a laser recirculator [69] increasing the repetition rate up to  $3.2 \cdot 10^3$  Hz were at the basis of the EuroGammas proposal for the ELI<sub>NP</sub> project [27]. The peculiar property of this

approach was that the high quality of the electron beam allowed to reduce the relative bandwidth down to  $3 \cdot 10^{-3}$ , satisfying the constraints of the nuclear photonics applications. The successive project for ELI\_NP, named VEGA [102], follows instead the same line as CLS. A plasma accelerator can also provide gamma rays using the fundamental or the second harmonics of the laser [103,104].

Table 4 shows the main parameters of few high-energy Compton sources.

**Table 4.** High energy ICS; all data are measured, apart the EuroGammas ones that are estimated.

ICS	Electron Energy (GeV)	$\lambda_{las}$ ( $\mu\text{m}$ )	Recoil	X Energy (MeV)	X/s	Rep Rate (Hz)	Bandwidth
UVSOR-III [30]	0.75	1.9–10.6	$<7.5 \cdot 10^{-3}$	1–5.4	$10^7$	$9 \cdot 10^7$	2.9%
New SUBARU [95]	0.5–1.5	1.06/0.532–10.5	$<5.2 \cdot 10^{-2}$	1–37	$1\text{--}4 \cdot 10^7$	$5 \cdot 10^8$	1.6%
LEPS/Leps2 [96]	8	0.26–0.35	0.6	$1.3\text{--}2.9 \cdot 10^3$	$10^6\text{--}10^7$	$5\text{--}50 \cdot 10^7$	
HIGs [12]	0.24–1	0.19–1.06	$<0.1$	1–100	$10^6\text{--}3 \cdot 10^{10}$	$5.6 \cdot 10^6$	1.5–3.5%
Euro-Gammas [27]	0.7	0.51	$2.7 \cdot 10^{-2}$	0.2–19.5	$5 \cdot 10^8$	100–36	0.3%

## 5. Conclusions

Inverse Compton scattering sources deliver sequences of picosecond long X or gamma-ray radiation pulses. The polarization of the emitted pulses can be linear, circular or elliptical, and can be completely controlled. The radiation is temporally shorter than synchrotron light sources, with a small and round size in the range of 10–80  $\mu\text{m}$ , allowing to exploit in phase contrast techniques the edge enhancement effect associated to the transverse coherence of the radiation beam. This is one of the key issues for advanced radiological imaging applications. Three main paradigms have been described: (i) RF Photo-injector generating high charge electron beams scattering a high energy density laser pulse, driving collisions at low repetition rate. (ii) Moderately high charge electron beam, generated at high repetition rate in Compact Storage Rings with mJ-class laser pulses stored in an optical Fabry-Perot Cavity, tightly focused. (iii) Low charge electron bunch delivered at very high repetition rate by a Super-Conducting RF Photo-Injector colliding with a mJ-class laser pulse stored in an optical Fabry-Perot Cavity (up to 1 MW stored laser power), focused at collision. The advantages of paradigm (i) are that it is possible to focus the electron beam below 20–30  $\mu\text{m}$ , due to the small beam emittance. Main drawback of paradigm (i) is the limitation in the repetition rate achievable, not larger than 100 Hz, in the present state of the art. Analogous limitations hold for the laser pulse, except for the possibility, not yet routinely exploited, of the use of a suitable recirculator. The electron energy, on the other hand, can be easily enhanced just by adding more RF accelerating structures allowing to exceed 20 MeV of gamma photon energy. The advantage of paradigm (ii) is the high repetition rate allowed by storing the electron beam in a ring. Limitations in focusing, mainly due to beam instabilities arising at such low energies (50 MeV), are intrinsic in this device. Energy upgrade is also an issue, since it involves the complete re-design of the machine. The implementation of pulsed operation is also difficult. The appealing characteristic of paradigm (iii) is the possibility to merge the operations typical of linacs such as dumping the beam after each collision at IP, with the high repetition rate typical of a storage ring (tens up to hundreds of MHz) thanks to the use of super-conducting RF cavities used to accelerate the electron beam. Another important advantage is the large sustainability permitted by the option of the energy recovery. The aim is to reach the largest radiation flux, with the lowest cost per photon. All the ICS projects has been conceived in the context of a broad spectrum inter-disciplinary large research infrastructure aiming at delivering advanced beams of electrons, photons, neutrons and positrons for basic and applied physics.

**Author Contributions:** Conceptualization, I.D., M.R., L.S. and V.P.; methodology, all authors; investigation, all authors; writing—original draft preparation, L.S. and V.P.; writing—review and editing, all authors. All authors have read and agreed to the published version of the manuscript.

**Funding:** This research received no external funding.

**Institutional Review Board Statement:** Not applicable.

**Informed Consent Statement:** Not applicable.

**Data Availability Statement:** Not applicable.

**Conflicts of Interest:** The authors declare no conflict of interest.

## Abbreviations

The following abbreviations are used in this manuscript:

ICS    Inverse Compton Scattering

## References

1. Bartzsch, S.; Oelfke, U. Line focus X-ray tubes—A new concept to produce high brilliance X-rays. *Phys. Med. Biol.* **2017**, *62*, 8600. <https://doi.org/10.1088/1361-6560/aa910b>.
2. Pogorelski, I.V.; Ben-Zvi, I.; Hirose, T.; Kashiwagi, S. Demonstration of  $8 \times 10^{18}$  photons/second peaked at 1.8 Å in a relativistic Thomson scattering experiment. *Phys. Rev. Spec. Top.-Accel. Beams* **2000**, *3*, 090702. <https://doi.org/10.1103/PhysRevSTAB.3.090702>.
3. Brown, W.; Anderson, S.; Barty, C.; Betts, S.; Booth, R.; Crane, J. Experimental characterization of an ultrafast Thomson scattering X-ray source with three-dimensional time and frequency-domain analysis. *Phys. Rev. Spec. Top.-Accel. Beams* **2004**, *7*, 060702. <https://doi.org/10.1103/PhysRevSTAB.7.060702>.
4. Albert, F.; Anderson, S.G.; Gibson, D.J.; Hagmann, C.A.; Johnson, M.S.; Messerly, M.; Semenov, V.; Shverdin, M.Y.; Rusnak, B.; Tremaine, A.M.; et al. Characterization and applications of a tunable, laser-based, MeV-class Compton-scattering ray source. *Phys. Rev. Spec. Top.-Accel. Beams* **2010**, *13*, 070704. <https://doi.org/10.1103/PhysRevSTAB.13.070704>.
5. Vaccarezza, C.; Alesini, D.; Anania, M.P.; Bacci, A.; Biagioni, A.; Bisesto, F.; Bellaveglia, M.; Cardarelli, P.; Cardelli, F. The SPARC\_LAB Thomson source. *Nucl. Instrum. Methods A* **2016**, *829*, 237–242. <https://doi.org/10.1016/j.nima.2016.01.089>.
6. Kuroda, R.; Toyokawa, H.; Sei, N.; Yasumoto, M.; Ogawa, H.; Koike, M.; Yamada, K.; Nakajyo, T.; Sakai, F.; Yanagida, T. Injector study for compact hard X-ray source via Laser Compton scattering. *Int. J. Mod. Phys. B* **2007**, *21*, 488–496. <https://doi.org/pros2.lib.unimi.it/10.1142/S0217979207042288>
7. Du, Y.; Yan, L.; Hua, J.; Du, Q.; Zhang, Z.; Li, R.; Qian, H.; Huang, W.; Chen, H.; Tang, C. Generation of first hard X-ray pulse at Tsinghua Thomson Scattering X-ray Source. *Rev. Sci. Instrum.* **2013**, *84*, 053301. <https://doi.org/10.1063/1.4803671>.
8. Bech, M.; Bunk, O.; David, C.; Ruth, R. Hard X-ray phase-contrast imaging with the Compact Light Source on inverse Compton X-rays. *J. Synchrotron Radiat.* **2009**, *16*, 43. <https://doi.org/10.1107/S090904950803464X>.
9. Eggl, E.; Dierolf, M.; Achterhold, K.; Jud, C.; Guenther, B.; Braig, E.; Gleich, B.; Pfeiffer, F. The Munich Compact Light Source: initial performance measures. *J. Synchrotron Radiat.* **2016**, *23*, 1137–1142. <https://doi.org/10.1107/S160057751600967X>.
10. Kraemer, J.M.; Jochmann, A.; Budde, M.; Bussmann, M.; Couperus, J.P.; Cowan, T.E. Making spectral shape measurements in inverse Compton scattering a tool for advanced diagnostic applications. *Sci. Rep.* **2018**, *8*, 1398. <https://doi.org/10.1038/s41598-018-19546-0>.
11. Powers, N.; Ghebregziabher, I.; Golovin, G. Quasi-monoenergetic and tunable X-rays from a laser-driven Compton light source. *Nat. Photonics* **2014**, *8*, 28–31. <https://doi.org/10.1038/nphoton.2013.314>.
12. Weller, H.R.; Ahmed, M.W.; Wu, Y.K. Nuclear Physics Research at the High Intensity Gamma-Ray Source (HIγS). *Nucl. Phys. News* **2015**, *25*, 19–24. <https://doi.org/10.1080/10619127.2015.1035932>.
13. Jochmann, A.; Irman, A.; Bussmann, M.; Couperus, J.P.; Cowan, T.E.; Debus, A.D.; Kuntzsch, M.; Ledingham, K.W.D.; Lehnert, U.; Sauerbrey, R.; et al. High Resolution Energy-Angle Correlation Measurement of Hard X Rays from Laser-Thomson Backscattering. *Phys. Rev. Lett.* **2013**, *111*, 114803. <https://doi.org/10.1103/PhysRevLett.111.114803>.
14. Babzien, M.; BenZvi, I.; Kusche, K.; Pavlishin, I.V.; Pogorelsky, I.V.; Siddons, D.P.; Yakimenko, V.; Cline, D.; Zhou, F.; Hirose, T.; et al. Observation of the Second Harmonic in Thomson Scattering from Relativistic Electrons. *Phys. Rev. Lett.* **2006**, *96*, 054802. <https://doi.org/10.1103/PhysRevLett.96.054802>.
15. Sakai, Y.; Pogorelsky, I.V.; Williams, O.; O’Shea, F.; Barber, S.; Gadjev, I.; Duris, J.; Musumeci, P.; Fedurin, M.; Korostyshevsky, A.; et al. Observation of redshifting and harmonic radiation in inverse Compton scattering. *Phys. Rev. Spec. Top.-Accel. Beams* **2015**, *18*, 060701. <https://doi.org/10.1103/PhysRevSTAB.18.060702>.
16. Sakai, Y.; Gadjev, I.; Hoang, P.; Majernik, N.; Nause, A.; Fukasawa, A.; Williams, O.; Fedurin, M.; Malone, B.; Swinson, C.; et al. Single shot, double differential spectral measurements of inverse Compton scattering in the nonlinear regime. *Phys. Rev. Accel. Beams* **2017**, *20*, 060701. <https://doi.org/10.1103/PhysRevAccelBeams.20.060701>.

17. Yan, W.; Fruhling, C.; Golovin, G.; Haden, D.; Luo, J.; Zhang, P.; Zhao, B.; Zhang, J.; Liu, C.; Chen, M.; et al. High-order multiphoton Thomson scattering. *Nat. Phot.* **2017**, *11*, 514–520. <https://doi.org/10.1038/nphoton.2017.100>.
18. Williams, O.; Andonian, G.; Babzien, M.; Hemsing, E.; Kusche, K.; Park, J.; Pogorelsky, I.V.; Priebe, G.; Rosenzweig, J.; Yakimenko, V. Characterization results of the BNL ATF Compton X-ray source using K-edge absorbing foils. *Nucl. Instrum. Methods A* **2009**, *608*, S18–S22. <https://doi.org/10.1016/j.nima.2009.05.166>.
19. Haden, D.; Golovin, G.; Yana, W.; Fruhling, C.; Zhang, P.; Zhao, B.; Banerjee, S.; Umstadter, D. High energy X-ray Compton spectroscopy via iterative reconstruction. *Nucl. Instrum. Methods A* **2020**, *951*, 163032. <https://doi.org/10.1016/j.nima.2019.163032>.
20. Chi, Z.; Du, Y.; Huang, W.; Tang, C. Linearly polarized X-ray fluorescence computed tomography based on a Thomson scattering light source: A Monte Carlo study. *J. Synchrotron Radiat.* **2020**, *27*, 737–745. <https://doi.org/10.1107/S1600577520003574>.
21. Fruhling, C.; Wang, J.; Umstadter, D.; Schulzke, C.; Romero, M.; Ware, M.; Peatross, J. Experimental observation of polarization-resolved nonlinear Thomson scattering of elliptically polarized light. *Phys. Rev. A* **2021**, *104*, 053519. <https://link.aps.org/doi/10.1103/PhysRevA.104.053519>.
22. Oliva, P.; Carpinelli, M.; Golosio, B.; Delogu, P.; Endrizzi, M.; Park, J.; Pogorelsky, I.V.; Yakimenko, V.; Williams, O.; Rosenzweig, J. Quantitative evaluation of single-shot inline phase contrast imaging using an inverse Compton X-ray source. *Appl. Phys. Lett.* **2010**, *97*, 134104. <https://doi.org/10.1063/1.3491430>.
23. Kuroda, R.; Toyokawa, H.; Yasumoto, M.; Ikeura-Sekiguchi, H.; Koike, M.; Yamada, K.; Yanagida, T.; Nakajyo, T.; Sakai, F.; Mori, K. Quasi-monochromatic hard X-ray source via laser Compton scattering and its application. *Nucl. Instrum. Methods A* **2011**, *637*, S183–S186. <https://doi.org/10.1016/j.nima.2010.04.001>.
24. Achterhold, K.; Bech, M.; Schleede, S.; Potdevin, G.; Ruth, R.; Loewen, R.; Pfeiffer, F. Monochromatic computed tomography with a compact laser-driven X-ray source. *Sci. Rep.* **2013**, *3*, 1313. <https://doi.org/10.1038/srep01313>.
25. Eggl, E.; Mechlem, K.; Braig, E.; Kulpe, S.; Dierolf, M.; Gunther, B.; Achterhold, K.; Herzen, J.; Gleich, B.; Rummeny, E.; et al. Mono-energy coronary angiography with a compact synchrotron source. *Sci. Rep.* **2017**, *7*, 42211. <https://doi.org/10.1038/srep42211>.
26. Amano, S.; Horikawa, K.; Ishihara, K.; Miyamoto, S.; Hayakawa, T.; Shizuma, T.; Mochizuki, T. Several-MeV  $\gamma$ -ray generation at NewSUBARU by laser Compton backscattering. *Nucl. Instrum. Methods A* **2009**, *602*, 337–341. <https://doi.org/10.1016/j.nima.2009.01.010>.
27. Adriani, O.; Albergo, S.; Alesini, D.; Anania, M.; Angal-Kalinin, D.; Antici, P.; Bacci, A.; Bedogni, R.; Bellaveglia, M.; Biscari, C.; et al. EuroGammaS: Technical Design Report for the ELI<sub>np</sub> Gamma beam System. *arXiv* **2014**, arXiv:1407.3669.
28. Dupraz, K.; Alkadi, M.; Alves, M.; Amoudry, L.; Auguste, D.; Babigeon, J.-L.; Baltazar, M.; Benoit, A.; Bonis, J.; Bonenfant, J.; et al. The ThomX ICS source. *Phys. Open* **2020**, *5*, 100051. <https://doi.org/10.1016/j.physo.2020.100051>.
29. Deitrick, K.; Hoffstaetter, G.H.; Franck, C.; Muraatori, B.D.; Williams, P.H.; Krafft, G.A.; Terzić, B.; Crone, J.; Owen, H. Intense monochromatic photons above 100 keV from an inverse Compton source. *Phys. Rev. Accel. Beams* **2021**, *24*, 050701. <https://doi.org/10.1103/PhysRevAccelBeams.24.050701>.
30. Zen, H.; Taira, Y.; Konomi, T.; Hayakawa, T.; Shizuma, T.; Yamazaki, J.; Kii, T.; Toyokawa, H.; Katoh, M.; Ohgaki, H. Generation of High Energy Gamma-ray by Laser Compton Scattering of 1.94-Pm Fiber Laser in UVSOR-III Electron Storage Ring. *Energy Procedia* **2026**, *89*, 335–345. <https://doi.org/10.1016/j.egypro.2016.05.044>.
31. Nagai, R.; Hajima, R.; Mori, M.; Shizuma, T.; Akagi, T.; Araki, S.; Honda, Y.; Kosuge, A.; Terunuma, N.; Urakawa, J. Demonstration of High-flux photon generation from an ERL-based laser Compton photon source. In Proceedings of the 6th International Particle Accelerator Conference IPAC2015, Richmond, VA, USA, 3–8 May 2015; ISBN 978-3-95450-168-7. <https://doi.org/10.18429/JACoW-IPAC2015-TUPJE002>.
32. Graves, W.S.; Bessuille, J.; Brown, P.; Carbajo, S.; Dolgashev, V.; Hong, K.-H.; Ihloff, E.; Khaykovich, B.; Lin, H.; Murari, K.; et al. Compact X-ray source based on burst-mode inverse Compton scattering at 100 kHz. *Phys. Rev. Spec. Top.-Accel. Beams* **2014**, *17*, 120701. <https://doi.org/10.1103/PhysRevSTAB.17.120701>.
33. Ainsworth, R.; Burt, G.; Konoplev, I.V.; Seryi, A. Asymmetric dual axis energy recovery linac for ultrahigh flux sources of coherent X-ray and THz radiation: Investigations towards its ultimate performance. *Phys. Rev. Spec. Top.-Accel. Beams* **2016**, *19*, 083502. <https://doi.org/10.1103/PhysRevAccelBeams.19.083502>.
34. bERLinPro Conceptual Design Report. Available online: [https://www.helmholtz-berlin.de/media/media/forschung/be/beschleuniger-ia/berlinpro\\_MAB/BPro\\_in\\_detail/Publications/bERLinPro\\_CDR.pdf](https://www.helmholtz-berlin.de/media/media/forschung/be/beschleuniger-ia/berlinpro_MAB/BPro_in_detail/Publications/bERLinPro_CDR.pdf) (accessed on 17 December 2022).
35. Faillace, L.; Agostino, R.G.; Bacci, A.; Barberi, R.; Bosotti, A.; Broggi, F.; Cardarelli, P.; Cialdi, S.; Drebot, I.; Formoso, V.; et al. Status of compact inverse Compton sources in Italy: BriXS and STAR SPIE Optical Engineering + Applications, 2019, San Diego, California, United States. *Proc. Adv. Lab.-Based X-ray Sources Opt. Appl. VII* **2019**, *11110*, 1111005. <https://doi.org/10.1117/12.2531168>.
36. Bacci, A.; Faillace, L.; Pellegrino, L.; Alesini, D.; Bini, S.; Cardelli, F.; Catuscelli, G.; Chiarelli, F.; Drebot, I.; Esposito, A.; et al. STAR HE-Linac Complete Detailed Design Report physics. *arXiv* **2021**, arXiv:2109.10351.
37. Cardarelli, P.; Bacci, A.; Calandrino, R.; Canella, F.; Castriconi, R.; Cialdi, S.; Del Vecchio, A.; di Franco, F.; Drebot, I.; Gambaccini, M.; et al. BriXS, a new X-ray inverse Compton source for medical applications. *Phys. Medica* **2020**, *77*, 127–137. <https://doi.org/10.1016/j.ejmp.2020.08.013>.
38. BriXSinO Conceptual Design Report. 2021. Available online: <https://marix.mi.infn.it/brixsino-docs/> (accessed on 10 May 2022).
39. Ghebregziabher, I.; Shadwick, B.A.; Umstadter, D. Spectral bandwidth reduction of Thomson scattered light by pulse chirping. *Phys. Rev. Spec. Top.-Accel. Beams* **2013**, *16*, 030705. <https://doi.org/10.1103/PhysRevSTAB.16.030705>.



40. Terzić, B.; Deitrick, K.; Hofler, A.; Krafft, G.A. Narrow-band emission in Thomson sources operating in the high-field regime. *Phys. Rev. Lett.* **2014**, *112*, 074801. <https://doi.org/10.1103/PhysRevLett.112.074801>.
41. Terzić, B.; Reeves, C.; Krafft, G.A. Combining harmonic generation and laser chirping to achieve high spectral density in Compton sources. *Phys. Rev. Spec. Top.-Accel. Beams* **2016**, *19*, 044403. <https://doi.org/10.1103/PhysRevAccelBeams.19.044403>.
42. Rykovanov, S.G.; Geddes, C.G.R.; Schroeder, C.B.; Esarey, E.; Leemans, W.P. Controlling the spectral shape of nonlinear Thomson scattering with proper laser chirping. *Phys. Rev. Spec. Top.-Accel. Beams* **2016**, *19*, 030701. <https://doi.org/10.1103/PhysRevAccelBeams.19.030701>.
43. Maroli, C.; Petrillo, V.; Drebot, I.; Serafini, L.; Terzić, B.; Krafft, G. A. Compensation of non-linear bandwidth broadening by laser chirping in Thomson sources. *J. Appl. Phys.* **2018**, *124*, 063105. <https://doi.org/10.1063/1.5033549>.
44. Terzić, B.; Krafft, G.; Brown, A.; Drebot, I.; Hagerman, T.; Johnson, E.; Krafft, G.A.; Maroli, C.; Petrillo, V.; Ruijter, M. Improving performance of inverse Compton sources through laser chirping. *Europhys. Lett.* **2019**, *126*, 12003. <https://doi.org/10.1209/0295-5075/126/12003>.
45. Seipt, D.; Kharin, V.Y.; Rykovanov, S.G. Optimizing Laser Pulses for Narrow-Band Inverse Compton Sources in the High-Intensity Regime. *Phys. Rev. Lett.* **2019**, *122*, 204802. <https://doi.org/10.1103/PhysRevLett.122.204802>.
46. Ruijter, M.; Petrillo, V.; Zepf, M. Decreasing the bandwidth of linear and nonlinear Thomson scattering radiation for electron bunches with a finite energy spread. *Phys. Rev. Accel. Beams* **2021**, *24*, 020702. <https://doi.org/10.1103/PhysRevAccelBeams.24.020702>.
47. Petrillo, V.; Drebot, I.; Krafft, G.; Maroli, C.; Rossi, A.R.; Rossetti Conti, M.; Ruijter, M.; Terzić, B. A laser frequency transverse modulation might compensate for the spectral broadening due to large electron energy spread in Thomson sources. *Photonics* **2022**, *9*, 62. <https://doi.org/10.3390/photronics9020062>.
48. Mackenroth, F.; Di Piazza, A.; Keitel, C.H. Determining the carrier-envelope phase of intense few-cycle laser pulses. *Phys. Rev. Lett.* **2010**, *105*, 063903. <https://doi.org/10.1103/PhysRevLett.105.063903>.
49. Ruijter, M.; Petrillo, V.; Teter, T.C.; Valialshchikov, M.; Rykovanov, S. Signatures of the Carrier Envelope Phase in Nonlinear Thomson Scattering. *Crystals* **2021**, *11*, 528. <https://doi.org/10.3390/cryst11050528>.
50. Schaap, B.H.; de Vos, T.D.C.; Smorenburg, P.W.; Luiten, O.J. Photon yield of superradiant inverse Compton scattering from microbunched electrons *New J. Phys.* **2022**, *24*, 033040. <https://doi.org/10.1088/1367-2630/ac59eb>.
51. Klein, R.; Kuske, P.; Thornagel, R.; Brandt, G.; Gorgen, R.; Ulm, G. Measurement of the BESSY II electron beam energy by Compton-backscattering of laser photons. *Nucl. Inst. Methods A* **2002**, *486*, 545–551. [https://doi.org/10.1016/S0168-9002\(01\)02162-3](https://doi.org/10.1016/S0168-9002(01)02162-3).
52. Fruhling, C.; Golovin, G.; Umstadter, D. Attosecond electron bunch measurement with coherent nonlinear Thomson scattering. *Phys. Rev. Accel. Beams* **2020**, *23*, 072802. <https://doi.org/10.1103/PhysRevAccelBeams.23.072802>.
53. Androsov, V.; Agafonov, A.; Bulyak, E.; Botman, J.I.M.; Grevtsev, V.; Gvozdenko, A.; Gladkikh, P.; Grigor'ev, Y.; Dovbnaya, A.; Drebot, I.; et al. Kharkov X ray generator NESTOR. In *Brilliant Light in Life and Material Sciences*; NATO Security through Science Series; Tsakanov, V., Wiedemann, H., Eds.; Springer: Dordrecht, The Netherlands, 2007. [https://doi.org/10.1007/978-1-4020-5724-3\\_8](https://doi.org/10.1007/978-1-4020-5724-3_8).
54. Miura, E.; Ishii, S.; Tanaka, K.; Kuroda, R.; Toyokawa, H. X-ray pulse generation by laser Compton 515 scattering using a high-charge, laser-accelerated, quasi-monoenergetic electron beam. *Appl. Phys. Express* **2014**, *7*, 046701. <https://doi.org/10.7567/APEX.7.046701>.
55. Akagi, T.; Kosuge, A.; Araki, S.; Hajima, R.; Honda, Y.; Miyajima, T.; Mori, M.; Nagai, R.; Nakamura, N.; Shimada, M.; et al. Narrow-band photon beam via laser Compton scattering in an energy recovery linac. *Phys. Rev. Spec. Top.-Accel. Beams* **2016**, *19*, 114701. <https://doi.org/10.1103/PhysRevAccelBeams.19.114701>.
56. Petrillo, V.; Bacci, A.; Drebot, I.; Opromolla, M.; Rossi, A.R.; Rossetti Conti, M.; Ruijter, M.; Samsam, S.; Serafini, L. Synchronised TeraHertz Radiation and Soft X-rays Produced in a FEL Oscillator. *Appl. Sci.* **2022**, *12*, 8341. <https://doi.org/10.3390/app12168341>.
57. Bacci, M.; Ferrario, C.; Maroli, V.; Petrillo, L. Serafini Transverse effects in the production of x rays with a free-electron laser based on an optical undulator. *Phys. Rev. Spec. Top.-Accel. Beams* **2006**, *9*, 060704.
58. Debus, A.D.; Bussmann, M.; Siebold, M.; Jochmann, A.; Schramm, U.; Cowan, T.E.; Sauerbrey, R. Traveling-wave Thomson scattering and optical undulators for high-yield EUV and X-ray sources. *Appl. Phys. Lasers Opt.* **2010**, *100*, 61–76. <https://doi.org/10.1007/s00340-010-3990-1>.
59. Drebot, I.; Petrillo, V.; Serafini, L. Two-colour X-gamma ray inverse Compton back-scattering source. *EPL* **2017**, *120*, 14002. <https://doi.org/10.1209/0295-5075/120/14002>.
60. Suerra, E.; Giannotti, D.; Canella, F.; Drebot, I.; Capra, S.; Cipriani, D.; Mettievier, D.; Galzerano, G.; Cardarelli, P.; Cialdi, S.; et al. A new method for spatial mode shifting of stabilized optical cavities for the generation of dual-color X-rays. *Nucl. Instrum. Methods A* **2021**, *1019*, 165852. <https://doi.org/10.1016/j.nima.2021.165852>.
61. Ranjan, N.; Terzić, B.; Krafft, G.A.; Petrillo, V.; Drebot, I.; Serafini, L. Simulation of inverse Compton scattering and its implications on the scattered linewidth. *Phys. Rev. Accel. Beams* **2018**, *21*, 030701. <https://doi.org/10.1103/PhysRevAccelBeams.21.030701>.
62. Curatolo, C.; Drebot, I.; Petrillo, V.; Serafini, L. Analytical description of photon beam phase spaces in inverse Compton scattering sources. *Phys. Rev. Accel. Beams* **2017**, *20*, 080701. <https://doi.org/10.1103/PhysRevAccelBeams.20.080701>.
63. Petrillo, V.; Bacci, A.; Curatolo, C.; Drebot, I.; Giribono, A.; Maroli, C.; Rossi, A.R.; Serafini, L.; Tomassini, P.; Vaccarezza, C.; et al. Polarization of x-gamma radiation produced by a Thomson and Compton inverse scattering. *Phys. Rev. Spec. Top.-Accel. Beams* **2015**, *18*, 110701. <https://doi.org/10.1103/PhysRevSTAB.18.110701>.
64. Tomassini, P.; Bacci, A.; Cary, J.; Ferrario, M.; Giulietti, A.; Giulietti, D.; Gizzi, L.A.; Labate, L.; Serafini, L.; Petrillo, V.; et al. Linear and nonlinear Thomson scattering for advanced X-ray sources in PLASMONX. *IEEE Trans. Plasma Sci.* **2008**, *36*, 1782–1789. <https://doi.org/10.1109/TPS.2008.927428>.

65. Boca, M.; Florescu, V. Thomson and Compton scattering with an intense laser pulse. *Eur. Phys. J. D* **2011**, *61*, 449. <https://doi.org/10.1140/epjd/e2010-10429-y>.
66. Maroli, C.; Petrillo, V.; Tomassini, P.; Serafini, L. Nonlinear effects in Thomson backscattering. *Phys. Rev. Spec. Top.-Accel. Beams* **2013**, *16*, 030706. <https://doi.org/10.1103/PhysRevSTAB.16.030706>.
67. Chen, S.; Maksimchuk, A.; Umstadter, D. Experimental observation of relativistic nonlinear Thomson scattering. *Nature* **1998**, *396*, 653–655. <https://doi.org/10.1038/25303>.
68. Petrillo, V.; Dattoli, G.; Drebot, I.; Nguyen, F. Compton Scattered X-Gamma Rays with Orbital Momentum. *Phys. Rev. Lett.* **2016**, *117*, 123903. <https://doi.org/10.1103/PhysRevLett.117.123903>.
69. Dupraz, K.; Cassou, K.; Delerue, N.; Fichot, P.; Martens, A.; Stocchi, A.; Variola, A.; Zomer, F.; Courjaud, A.; Mottay, E.; et al. Design and optimization of a highly efficient optical multipass system for  $\gamma$ -ray beam production from electron laser beam Compton scattering. *Phys. Rev. Spec. Top.-Accel. Beams* **2014**, *17*, 033501. <https://doi.org/10.1103/PhysRevSTAB.17.033501>.
70. Ovodenko, A.; Agustsson, R.; Babzien, M.; Campese, T.; Fedurin, M.; Murokh, A.; Pogorelsky, I.; Polyanskiy, M.; Rosenzweig, J.; Sakai, Y.; et al. High duty cycle inverse Compton scattering X-ray source. *Appl. Phys. Lett.* **2016**, *109*, 253504. <https://doi.org/10.1063/1.4972344>.
71. Chi, Z.; Yan, L.; Zhang, Z.; Zhou, Z.; Zheng, L.; Wang, D.; Tian, Q.; Wang, W.; Nie, Z.; Zhang, J.; et al. Diffraction based method to reconstruct the spectrum of the Thomson scattering X-ray source. *Rev. Sci. Instrum.* **2017**, *88*, 045110. <https://doi.org/pros2.lib.unimi.it/10.1063/1.4981131>.
72. Golosio, B.; Endrizzi, M.; Oliva, P.; Delogu, P.; Carpinelli, M.; Pogorelski, I.; Yakimenko, V. Measurement of an inverse Compton scattering source local spectrum using k-edge filters. *Appl. Phys. Lett.* **2012**, *100*, 164104. <https://doi.org/10.1063/1.4703932>.
73. Hongze, Z. Experiments on Polarization Control of Thomson Scattering X/ $\gamma$ -ray Source. In Proceedings of the 13th Symposium on Accelerator Physics SAP2017, Jishou, China, 28–30 August 2017; ISBN 978-3-95450-199-1. <https://doi.org/10.18429/JACoW-SAP2017-WEBH3>
74. Feng, B.; Qin, C.Y.; Geng, X.S.; Yu, Q.; Wang, W.Q.; Wu, Y.T.; Yan, X.; Ji, L.L.; Shen, B.F. The emission of  $\gamma$ -Ray beams with orbital angular momentum in laser-driven micro-channel plasma target. *Sci. Rep.* **2019**, *9*, 18780. <https://doi.org/pros2.lib.unimi.it/10.1038/s41598-019-55217-4>.
75. Fujii, T.; Fukuyama, N.; Tanaka, C.; Ikeya, Y.; Shinozaki, Y.; Kawai, T.; Atsumi, T.; Shiraiishi, T.; Sato, E.; Kuroda, R.; et al. Visualization of microvessels by angiography using inverse-Compton scattering X-rays in animal models. *J. Synchrotron Radiat.* **2014**, *21*, 1327–1332. <https://doi.org/10.1107/S1600577514017500>.
76. Ikeura-Sekiguchi, H.; Kuroda, R.; Yasumoto, M.; Toyokawa, H.; Koike, M.; Yamada, K.; Sakai, F.; Mori, K.; Maruyama, K.; Oka, H.; et al. In-line phase-contrast imaging of a biological specimen using a compact laser-Compton scattering-based X-ray source. *Appl. Phys. Lett.* **2008**, *92*, 131107. <https://doi.org/10.1063/1.2903148>.
77. Schleede, S.; Meinel, F.G.; Bech, M.; Herzen, J.; Achterhold, K.; Potdevin, G.; Malecki, A.; Adam-Neumair, S.; Thieme, S.F.; Bamberg, F.; et al. Emphysema diagnosis using X-ray dark-field imaging at a laser-driven compact synchrotron light source. *Proc. Natl. Acad. Sci. USA* **2012**, *109*, 17880–17885. <https://doi.org/10.1073/pnas.1206684109>.
78. Meinel, F.G.; Schwab, F.; Schleede, S.; Bech, M.; Herzen, J.; Achterhold, K.; Auweter, S.; Bamberg, F.; Yildirim, A.O.; Bohla, A.; et al. Diagnosing and mapping pulmonary emphysema on X-ray projection images: incremental value of grating-based X-ray dark-field imaging. *PLoS ONE* **2013**, *8*, 59526. <http://dx.doi.org/10.1371/journal.pone.0059526>.
79. Abendroth, J.; McCormick, M.S.; Edwards, T.E.; Staker, B.; Loewen, R.; Gifford, M.; Rifkin, J.; Mayer, C.; Guo, W.; Zhang, Y.; et al. X-ray structure determination of the glycine cleavage system protein H of Mycobacterium tuberculosis using an inverse Compton synchrotron X-ray source. *J. Struct. Funct. Genom.* **2010**, *11*, 91–100. <https://doi.org/10.1007/s10969-010-9087-6>.
80. Eggel, E.; Schleede, S.; Bech, M.; Achterhold, K.; Loewen, R.; Ruth, R.D.; Pfeiffer, F. X-ray phase-contrast tomography with a compact laser-driven synchrotron source. *Proc. Natl. Acad. Sci. USA* **2015**, *112*, 5567–5572. <https://doi.org/10.1073/pnas.1500938112>.
81. Gromann, L.B.; De Marco, F.; Willer, K.; Noël, P.B.; Scherer, K.; Renger, B.; Gleich, B.; Achterhold, K.; Fingerle, A.A.; Muenzel, D.; et al. In-vivo X-ray Dark-Field Chest Radiography of a Pig. *Sci. Rep.* **2017**, *7*, 4807. <https://doi.org/10.1038/s41598-017-05101-w>.
82. Gradl, R.; Dierolf, M.; Yang, L.; Hehn, L.; Günther, B.; Möller, W.; Kutschked, D.; Stoeger, T.; Gleich, B.; Achterhold, K.; et al. Visualizing treatment delivery and deposition in mouse lungs using in vivo X-ray imaging. *J. Control. Release* **2019**, *307*, 282–291. <https://doi.org/10.1016/j.jconrel.2019.06.035>.
83. Willer, K.; Fingerle, A.A.; Gromann, L.B.; De Marco, F.; Herzen, J.; Achterhold, K.; Gleich, B.; Muenzel, D.; Scherer, K.; Renz, M.; et al. X-ray dark-field imaging of the human lung—A Feasibility study on a deceased body. *PLoS ONE* **2019**, *13*, 0204565. <https://doi.org/10.1371/journal.pone.0204565>.
84. Huang, J.; Günther, B.; Achterhold, K.; Cui, Y.; Gleich, B.; Dierolf, M.; Pfeiffer, F. Energy-Dispersive X-ray Absorption Spectroscopy with an Inverse Compton Source. *Sci. Rep.* **2020**, *10*, 8772. <https://doi.org/10.1038/s41598-020-65225-4>.
85. Kulpe, S.; Dierolf, M.; Braig, E.-M.; Guenther, B.; Achterhold, K.; Gleich, B.; Herzen, J.; Rummeny, E.; Pfeiffer, F.; Pfeiffer, D. K-edge subtraction imaging for iodine and calcium separation at a compact synchrotron X-ray source. *J. Med. Imaging* **2020**, *7*, 023504. <https://doi.org/10.1117/1.JMI.7.2.023504>.
86. Dombrowsky, A.C.; Burger, K.; Porth, A.-K.; Stein, M.; Dierolf, M.; Günther, B.; Achterhold, K.; Gleich, B.; Feuchtinger, A.; Bartzsch, S.; et al. A proof of principle experiment for microbeam radiation therapy at the Munich compact light source. *Radiat. Environ. Biophys.* **2020**, *59*, 111–120. <https://doi.org/10.1007/s00411-019-00816-y>.

87. Tigner, M. A Possible Apparatus for Electron Clashing-Beam Experiments. *Nuovo Cim.* **1965**, *37*, 1228–1231. <https://doi.org/10.1007/BF02773204>.
88. Sannibale, F.; Filippetto, D.; Qian, H.; Mitchell, C.E.; Feng, J.; Harris, G.; Johnson, M.J.; Kramasz, T.D.; Leitner, D.; Nasiatka, J.R.; et al. APEX phase-II commissioning results at the Lawrence Berkeley National Laboratory. In Proceedings of the 7th International Particle Accelerator Conference, IPAC 2016, Busan, Republic of Korea, 8–13 May 2016; pp. 1041–1043, ISBN 978-395450147-2.
89. Kayran, D. *Status and Commissioning Results of the R and D ERL at BNL*; Tech. Rep.; Brookhaven National Laboratory (BNL): Upton, NY, USA, 2015.
90. Toyokawa, H.; Ohgaki, H.; Hayakawa, T.; Kii, T.; Shizuma, T.; Hajima, R.; Kikuzawa, N.; Masuda, K.; Kitatani, F.; Harada, H. Two-Dimensional Isotope Imaging of Radiation Shielded Materials Using Nuclear Resonance Fluorescence. *Jpn. J. Appl. Phys.* **2011**, *50*, 100209. <https://doi.org/10.1143/JJAP.50.100209>.
91. Kulikov, O.F.; Telnov, Y.Y.; Filippov, E.I.; Yakimenko, M.N. Compton effect on moving electrons. *Phys. Lett.* **1964**, *13*, 344–346. [https://doi.org/10.1016/0031-9163\(64\)90040-X](https://doi.org/10.1016/0031-9163(64)90040-X).
92. Kawase, K.; Arimoto, Y.; Fujiwara, M.; Okajima, S.; Shoji, M.; Suzuki, S.; Tamura, K.; Yorita, T.; Ohkuma, H. MeV  $\gamma$ -ray generation from backward Compton scattering at SPring-8. *Nucl. Instrum. Meth. A* **2008**, *592*, 154. <https://doi.org/10.1016/J.NIMA.2008.04.008>.
93. Litvinenko, V.N.; Madey, J.M.J. Intense Compton y-ray source from the Duke storage ring FEL. *Nucl. Inst. Methods A* **1996**, *375*, 580–583. [https://doi.org/10.1016/0168-9002\(95\)01358-X](https://doi.org/10.1016/0168-9002(95)01358-X).
94. Aoki, K.; Hosono, K.; Hadame, T.; Munenaga, H.; Kinoshita, K.; Toda, M.; Amano, S.; Miyamoto, S.; Mochizuki, T.; Aoki, M.; et al. High-energy photon beam production with laser-Compton backscattering. *Nucl. Inst. Methods A* **2004**, *516*, 228–236. <https://doi.org/10.1016/J.NIMA.2003.08.153>.
95. Horikawa, K.; Miyamoto, S.; Amano, S.; Mochizuki, T. Measurements for the energy and flux of Compton scattering  $\gamma$ -ray photons generated in an electron storage ring: New SUBARU. *Nucl. Inst. Methods A* **2010**, *618*, 209–215. <https://doi.org/10.1016/j.nima.2010.02.259>.
96. Muramatsu, N.; Kon, Y.; Daté, S.; Ohashi, Y.; Akimune, H.; Chen, J.Y.; Fujiwara, M.; Hasegawa, S.; Hotta, T.; Ishikawa, T.; et al. Development of high intensity laser-electron photon beams up to 2.9 GeV at the spring-8 LEPS beamline. *Nucl. Inst. Methods A* **2014**, *737*, 184–194. <http://dx.doi.org/10.1016/j.nima.2013.11.039>.
97. Muramatsu, N.; Yosoi, M.; Yorita, T.; Ohashi, Y.; Ahn, J.K.; Ajimura, S.; Asano, Y.; Chang, W. C.; Chen, J.Y.; Daté, S. SPring-8 LEPS2 beamline: A facility to produce a multi-GeV photon beam via laser Compton scattering. *Nucl. Inst. Methods A* **2022**, *1033*, 166677. <https://doi.org/10.1016/j.nima.2022.166677>.
98. Nutarelli, D.; Couprie, M.E.; Nahon, L.; Bakker, R.; Delboulbe, A.; Roux, R.; Visentin, B.; Billardon, M. Gamma rays production by intra-cavity Compton Back Scattering with Super-ACO Storage Ring Free Electron Laser. *Nucl. Inst. Methods A* **1998**, *407*, 459–463. [https://doi.org/10.1016/S0168-9002\(98\)00068-0](https://doi.org/10.1016/S0168-9002(98)00068-0).
99. Hosaka, M.; Hama, H.; Kimura, K.; Yamazaki, J.; Kinoshita, T. Observation of intracavity Compton backscattering of the UVSOR free electron laser. *Nucl. Inst. Methods A* **1997**, *393*, 525–529. [https://doi.org/10.1016/S0168-9002\(97\)00563-9](https://doi.org/10.1016/S0168-9002(97)00563-9).
100. Kaneyasu, T.; Takabayashi, Y.; Iwasaki, Y.; Koda, S. Generation of laser Compton gamma-rays in SAGA light source. *Nucl. Inst. Methods A* **2011**, *659*, 30–35. <https://doi.org/10.1016/j.nima.2011.08.047>.
101. Litvinenko, V.N.; Burnham, B.; Emamian, M.; Hower, N.; Madey, J.M.J.; Morcombe, P.; O’Shea, P.G.; Park, S.H.; Sachtschale, R.; Straub, K.D.; et al. Gamma-Ray Production in a Storage Ring Free-Electron Laser. *Phys. Rev. Lett.* **1997**, *78*, 4569. <https://doi.org/10.1103/PhysRevLett.78.4569>.
102. VEGA Project. Available online: <https://www.innovationnewsnetwork.com/eli-np-revealing-intimate-structure-matter-extreme-light/18383/> (accessed on 27 December 2022).
103. Chen, S.; Powers, N.D.; Ghebregziabher, I.; Maharjan, C.M.; Liu, C.; Golovin, G.; Banerjee, S.; Zhang, J.; Cunningham, N.; Moorti, A.; et al. MeV-energy X rays from inverse compton scattering with laser-wakefield accelerated electrons. *Phys. Rev. Lett.* **2013**, *110*, 155003. <https://doi.org/10.1103/PhysRevLett.110.155003>.
104. Liu, C.; Golovin, G.; Chen, S.; Liu, C.; Golovin, G.; Chen, S.; Zhang, J.; Zhao, B.; Haden, D.; Banerjee, S.; et al. Generation of 9 MeV  $\gamma$ -rays by all-laser-driven Compton scattering with second-harmonic laser light. *Opt. Lett.* **2014**, *39*, 4132–4135. <https://doi.org/10.1364/OL.39.004132>.

**Disclaimer/Publisher’s Note:** The statements, opinions and data contained in all publications are solely those of the individual author(s) and contributor(s) and not of MDPI and/or the editor(s). MDPI and/or the editor(s) disclaim responsibility for any injury to people or property resulting from any ideas, methods, instructions or products referred to in the content.